POLITECNICO DI TORINO
Repository ISTITUZIONALE

3D printed electrolyte-supported solid oxide cells based on Ytterbium-doped scandia-stabilized zirconia

Original
3D printed electrolyte-supported solid oxide cells based on Ytterbium-doped scandia-stabilized zirconia / Márquez, S., Anelli, S., Nuñez, M., Lira, M., Maria Asensio, A., Torrell, M., Tarancón, A.. - In: JPHYS ENERGY. - ISSN 2515-7655. - 6:1(2024). [10.1088/2515-7655/ad17e3]

Availability:
This version is available at: 11583/2996704 since: 2025-01-20T13:47:00Z

Publisher:
Institute of Physics

Published
DOI:10.1088/2515-7655/ad17e3

Terms of use:

This article is made available under terms and conditions as specified in the corresponding bibliographic description in the repository

Publisher copyright

(Article begins on next page)

27 June 2026

JPhys Energy

PURPOSE-LED PUBLISHING™

PAPER • OPEN ACCESS

3D printed electrolyte-supported solid oxide cells based on Ytterbium-doped scandia-stabilized zirconia

To cite this article: Santiago Márquez *et al* 2024 *J. Phys. Energy* **6** 015016

View the article online for updates and enhancements.

You may also like

- Oxygen Reduction, Transport and Separation in Low Silver Content Scandia-Stabilized Zirconia Composites
E Ruiz-Trejo, A. Bertei, A. Maserati et al.
- Fabrication and Evaluation of a Micro-Tubular Solid Oxide Fuel Cell with an Inert Support Using Scandia-Stabilized Zirconia Electrolyte
Dhruba Panthi, Bokkyu Choi and Atsushi Tsutsumi
- Evaluation of Micro LSM-Supported GDC/ScSZ Bilayer Electrolyte with LSM–GDC Activation Layer for Intermediate Temperature-SOFCs
Toshiaki Yamaguchi, Sota Shimizu, Toshio Suzuki et al.

This content was downloaded from IP address 130.192.43.106 on 22/01/2025 at 08:57

Journal of Physics: Energy

PAPER

3D printed electrolyte-supported solid oxide cells based on Ytterbium-doped scandia-stabilized zirconia

Santiago Márquez[1], Simone Anelli[1,2], Marc Nuñez[1], Maritta Lira[1], Antonio Maria Asensio[1], Marc Torrell[1,*] and Albert Tarancón[1,3,*]

[1] IREC, Catalonia Institute for Energy Research, Jardins de les Dones de Negre 1, 2 a pl, 08930 Sant Adrià de Besòs, Barcelona, Spain
[2] Department of Applied Science and Technology (DISAT), Politecnico di Torino, 10129 Torino, Italy
[3] ICREA, Passeig Lluís Companys 23, 08010 Barcelona, Spain
[*] Authors to whom any correspondence should be addressed.

E-mail: mtorrell@irec.cat and atarancon@irec.cat

OPEN ACCESS

RECEIVED
16 October 2023

REVISED
27 November 2023

ACCEPTED FOR PUBLICATION
21 December 2023

PUBLISHED
8 January 2024

Original content from this work may be used under the terms of the Creative Commons Attribution 4.0 licence.

Any further distribution of this work must maintain attribution to the author(s) and the title of the work, journal citation and DOI.

Keywords: SOFC, SOEC, SLA, 3D printing, ceramics, stereolitography, 6Yb4ScSZ

Supplementary material for this article is available online

Abstract

Solid oxide cells (SOC) are an efficient and cost-effective energy conversion technology able to operate reversibly in fuel cell and electrolysis mode. Electrolyte-supported SOC have been recently fabricated employing 3D printing to generate unique geometries with never-explored capabilities. However, the use of the state-of-the-art electrolyte based on yttria-stabilized zirconia limits the current performance of such printed devices due to a limited oxide-ion conductivity. In the last years, alternative electrolytes such as scandia-stabilized zirconia (ScSZ) became more popular to increase the performance of electrolyte-supported cells. In this work, stereolithography 3D printing of Ytterbium-doped ScSZ was developed to fabricate SOC with planar and corrugated architectures. Symmetrical and full cells with about 250 μm- thick electrolytes were fabricated and electrochemically characterized using impedance spectroscopy and galvanostatic studies. Maximum power density of 500 mW cm^{-2} in fuel cell mode and an injected current of 1 A cm^{-2} at 1.3 V in electrolysis mode, both measured at 900 °C, were obtained demonstrating the feasibility of 3D printing for the fabrication of high-performance electrolyte-supported SOC. This, together with excellent stability proved for more than 350 h of operation, opens a new scenario for using complex-shaped SOC in real applications.

1. Introduction

Global warming is boosting political and scientific efforts to reduce CO_2 emissions for minimizing the greenhouse effect [1]. In this regard, a massive deployment of renewable energy sources such as hydroelectric, wind, solar, and biogas is expected in the forthcoming years [2]. However the intermittent nature of renewable energy sources and their production mismatch with the energy demand poses significant challenges to their widespread adoption [3]. To be effectively deployed, the implementation of seasonal and efficient energy storage systems is required. Among other technologies such as batteries or supercapacitors, hydrogen has emerged as a promising energy vector for efficient chemical storage from renewable electricity garnering substantial attention in recent years [4–6]. Currently, the majority (95%) of the world's hydrogen production, 95 Mt yr^{-1} [7], is based on steam methane reforming, which results in more than 12 Kg of CO_2 emitted per kilogram of produced hydrogen [2, 8]. However, there are alternative methods for hydrogen production with no CO_2 associated emissions, the so-called green hydrogen, such as thermochemical water splitting [9], and photocatalytic water splitting [10], being the latest and most mature and efficient route [11]. Nowadays, there are three main technologies for green hydrogen production based on water electrolysis, which are basically differentiated by their electrolyte ion conduction mechanism and operation

© 2024 The Author(s). Published by IOP Publishing Ltd

temperature. These technologies are proton exchange membrane [12], alkaline electrolysis [13], and solid oxide electrolysis [14]. All these technologies and devices can reversibly work in fuel cell mode, converting hydrogen into electricity. Solid oxide cells (SOC) offer several advantages over proton exchange or alkaline cells due to their operation at high temperatures, typically above 750 °C presenting faster reaction kinetics and thermodynamic advantages, resulting in higher power densities and improved overall performance and efficiency. With an impressive energy conversion efficiency of up to 80%, SOC technologies demonstrate their potential as highly efficient energy storage and conversion systems [15].

SOC devices consist typically of two porous electrodes and a dense oxide-ion electrolyte [16]. The state-of-the-art electrolyte material for SOC applications is yttria-stabilized zirconia (YSZ) [17]. However, due to a limited conductivity, YSZ is often substituted by a more conductive scandia-stabilized zirconia (ScSZ) in electrolyte-supported cell (ESC) configurations, where a minimum thickness of 100–150 μm is typically required [18]. Despite the interest of ScSZ as a substitute for YSZ in ESCs, the cubic phase of ScSZ presents certain instabilities under operation in the long term (especially in SOEC mode), giving rise to the formation of less conductive non-cubic domains [19]. This problem can be partially solved by doping ScSZ with Yb, which improves the long term durability while keeping a reasonable conductivity above YSZ [11, 20, 21]. The level of Yb doping can be tailored for specific performance requirements, being $(ZrO_2)_{0.9}(Yb_2O_3)_{0.06}(Sc_2O_3)_{0.04}$ (6Yb4ScSZ) a good trade-off for both conductivity and durability for operation in SOFC and SOEC modes [22].

Regarding SOC electrodes, referred to as the fuel and oxygen electrodes, composites made of electrode and electrolyte materials are typically the choice to meet the various requirements for an optimal performance, which include a balance of ionic and electronic conductivity, structural stability, catalytic activity, and porosity for gas passage within the electrode [23]. In particular, the optimization of the triple-phase boundary (TPB) length, where gases, electronic conductive and ionic conductive phases meet, is essential for an efficient electrochemical performance [24, 25]. In the case of oxygen electrodes, perovskite oxides based on manganese, cobalt, or iron are typical choices. In particular, lanthanum strontium manganite (LSM) exhibits high processing stability at around 1200 °C and good catalytic activity while lanthanum strontium cobalt ferrite with mixed ionic-electronic conductivity improves the TPB efficiency [26]. On the other side, fuel electrodes are typically made of ceramic-metal composites that combine metallic Ni and YSZ (Ni-YSZ), which present excellent catalytic activity and electrical conductivity and mechanical stability and ionic conductivity, respectively [27].

Regarding manufacturing of SOCs, conventional techniques are employed limiting the available geometries to planar and tubular configurations fabricated by tape casting or screen printing and extrusion, respectively [28–31]. Recently, 3D printing of ceramics has been proposed as an alternative to conventional manufacturing techniques for SOC fabrication [32]. Among other approaches, the authors have successfully used stereolithography (SLA) 3D printing to produce YSZ electrolytes for SOC applications [33, 34]. Despite the potential benefits of using SLA in SOCs, the minimum achievable thickness and the reduced availability of printable materials is still hampering the impact of the technology.

In this study, a printable feedstock for SLA of 6Yb4ScSz has been developed in order to fabricate SOC with planar and high-aspect ratio corrugated structures using LSM–YSZ/6Yb4ScSz/Ni–YSZ materials. After fabrication and characterization, a comprehensive analysis of the electrochemical performance of both types of cells from 800 °C to 900 °C, considering fuel cell and electrolysis operation modes was carried out. Employing electrochemical impedance spectroscopy (EIS), it is possible to identify the underlying factors contributing to this enhancement in performance. Finally, mid-term operation in galvanostatic SOFC mode was carried out for more than 500 h.

2. Experimental method

2.1. Preparation of the SLA 6Yb4ScSZ slurry

The printable UV-curable slurry was composed of: trimethylolpropane triacrylate (TMPTA, supplied by Sigma–Aldrich, Germany) as a monomer, polyethylene glycol 400 (PEG-400, supplied by Sigma–Aldrich, Germany) as a plasticizer, Monofax (supplied by Sigma-Aldrich, Germany) as a dispersant, 2,2-Dimethoxy-2-phenylacetophenone (supplied by Sigma-Aldrich, Germany) as a photoinitiator active at 355 nm and the ceramic powder of 6Yb4ScSZ with formula $(ZrO_2)_{0.9}(Yb_2O_3)_{0.06}(Sc_2O_3)_{0.04}$ (KCeracell Fuel and electrochemical materials, South Korea D50 = 0.314 μm). The proportion of ceramic loading in the slurry as well as the rest of the compounds can be found in table 1.

The 6Yb4ScSZ powder was dried before mixing with the other components of the organic vehicle. The UV-resin was prepared by mixing the components one by one in a planetary mixer (ARE-250 CE THINKY, USA). Firstly, the organic part was mixed at 1400 rpm min^{-1}. The solid loading was added in 4 steps at 1400 rpm min^{-1}.

Table 1. Composition in %vol of all the components of the formulated slurry.

Material	Composition (% vol)
6Yb4ScSZ	47
TMPTA	45
PEG-400	2.6
Monofax	4.9
2,2-Dimethoxy-2-phenylacetophenone	0.5

Aiming to determine the rheological properties and the printability of the formulated slurry, a rheological characterization was performed with a DHR-2 rheometer (TA Instruments, Waters, USA). The measurements were carried out using a plate-to-plate geometry, the temperature was maintained in all cases at 25 °C.

2.2. Fabrication of symmetrical and complete cells

6Yb4ScSZ printed parts with a diameter of ca. 2.5 cm were produced using a big format industrial ceramic SLA 3D printer (CERAMAKER 900 3DCERAM, France). For all the prints in this work, 25 μm thick layers were deposited with curing power laser density of 220 mW cm^{-2} (355 nm laser wavelenght), laser spot size of 40 μm, and laser speed of 860 cm s^{-1} for the marking step. The green cells were cleaned using commercial solution (Ceraclean, 3D Ceram, France) and placed in an oven at 60 °C for 168 h, in order to remove the excess of cleaning solution. The green printed electrolytes, planar and corrugated, were thermally treated for more than 75 h in nitrogen (N_2) to eliminate the organics present on the slurry and sintered in air at 1400 °C for 2 h to ensure densification of the ceramic electrolyte. All thermal treatments were carried out in a tubular furnace (ST 16 85 45, Hobersal, Spain). After sintering the electrolyte, LSM-YSZ composite electrodes (Fuel cell materials, USA) were deposited on both sides for the fabrication of symmetrical cells. Optimization of the attachment temperature of the LSM-YSZ electrode was carried out at three different attachment temperatures 1100, 1150, and 1200 °C (at a ramp rate of 2 C° min^{-1} for 2 h). Similarly, NiO-YSZ inks (Fuel cell materials, USA) were employed to fabricate the fuel electrode. After air spraying the electrode, thermal treatment at 1400 °C for 2 h was carried out in air atmospheres.

Thermogravimetric analysis (TGA) and differential Scanning Calorimetry (DSC) (Mettler Toledo, TGA: TGA/DSC1 DSC: DSC3) were used to design an optimal debinding and sintering cycle of the printed parts. The DSC and TGA were operated under inert atmosphere of N_2 from 25 °C to 600 °C for the DSC and from 25 °C to 800 °C for the TGA.

2.3. Electrochemical characterization of SOC symmetric and complete cells

EIS measurements of the fabricated LSM-YSZ/6Yb4ScSZ/LSM-YSZ symmetrical cells were carried out in the temperature range of 500 °C–900 °C under air, using homemade automatic test benches based on commercial Probostat test stations (NOR- ECS, Norway). Equivalent circuits were employed to fit the EIS results. The equivalent circuit consisted of an inductance (L) for the contribution of the setup, a serial resistance R_s, including all the ohmic contributions (e.g. the electrolyte), and two (RQ) elements for the symmetrical electrodes.

The electrochemical characterization of the complete cells was performed by *I–V* polarization curves (galvanostatic mode) and EIS measurements. The full electrochemical characterization of the SOCs was measured at 800 °C, 850 °C, and 900 °C with a galvanostat/potenciostat and frequency response analyzer (Parstat 2273, PAR, USA). Ceramabond (Aremco) was used to seal the cell and isolate the reducing and oxidizing atmospheres. For the gas control and monitoring during the SOFC and SOEC tests (H_2, Air, and Steam), as well as during the characterization of the symmetrical cells (synthetic air), computer-controlled mass flows from Bronkhorst was utilized (Bronk–horst, Netherlands).

Morphological and microstructural characterization was performed using scanning electron microscopy (SEM) (AURIGA with Gemini 30kV FESEM column from ZEISS).

3. Results

3.1. Optimization of the fabrication process and fabrication of the cells

In order to evaluate the printability of the developed slurries, a characterization of the apparent viscosity and the shear stress as a function of the shear rate was carried out (figure 1(a)). Viscosity values of 90 Pa s at the working share rate of 100 s^{-1} (similar to the one applied during the doctor blade step within the 3D printer) were obtained. This rheological behavior is considered adequate for a good printability of the slurry (as compared in figure 1(a) with a commercial reference slurry (ZR8-F01, 3DCERAM, France) with excellent

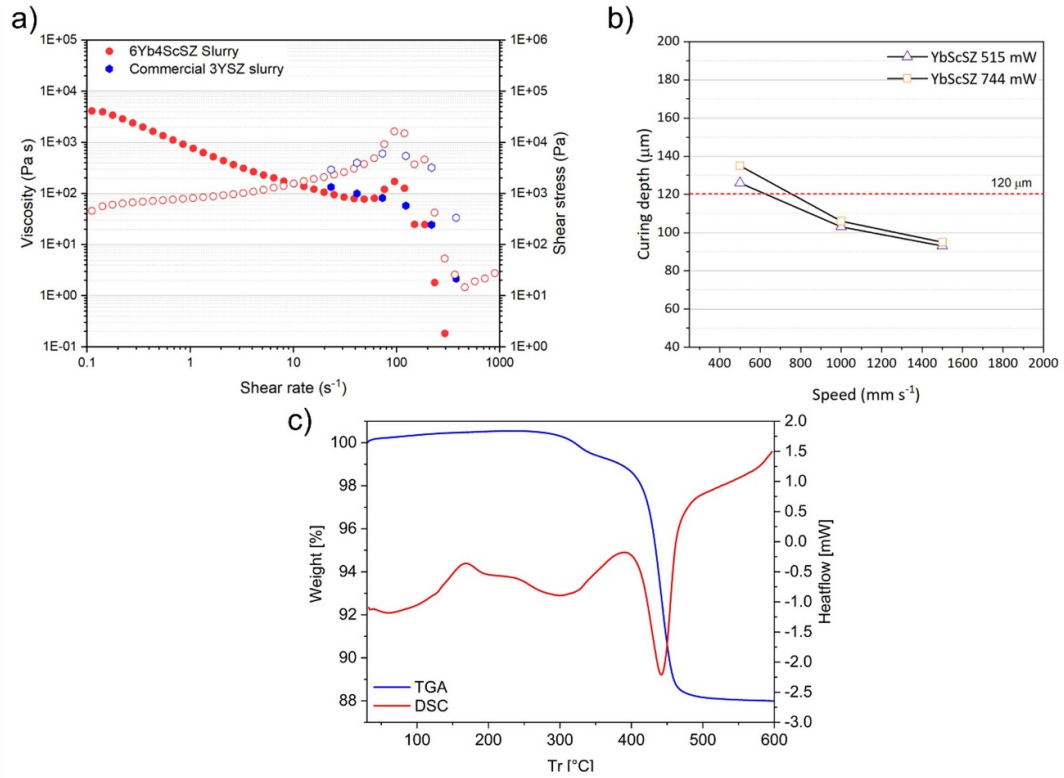

Figure 1. (a) Apparent viscosity (Pa s) vs Share rate (s–1) and Share stress (Pa) vs Share stress of the 6YbScSz formulated slurry (b) cure depth test of the produced paste of 6Yb4ScSz (c) TGA and DSC results for the photocurable 6Yb4ScSZ samples as a function of temperature.

printability). Beyond the rheological characterization, the printable slurry should present a minimum curing depth to ensure the good interlayer attachment. In this particular case, the target curing depth is 120 μm, equivalent to the thickness of four printed layers. Figure 1(c) shows the results of the polymerization performed to the printed slurry with different laser power (744 and 515 mW) and laser speed (500–1500 mm s^{-1}). Curing depths of 125 μm at 515 mW and 500 mm s^{-1} and 136 μm at 744 and 500 mm s^{-1} reaching the required conditions for a proper printing.

Finally, TGA and DSC analyses were performed to determine the best thermal process for carrying out the debinding and sintering processes dedicated to the removal of the organics and sintering of the printed part, respectively. Figure 1(d) shows the TGA-DSC curves used to determine the relevant temperatures for the debinding treatment. The obtained information allows tuning the temperature profile of the debinding process in order to avoid cracks and defects on the final piece. Observed weight losses in the temperature range of 90 °C–350 °C can be attributed to the evaporation of solvents and the organic additives present. The cumulative weight loss during this stage is around ≈2% mass. Considering this value one can attribute it to the combined contribution of diluent, dispersant, and photoinitiator. The DSC exhibited a distinct endothermic peak at ≈430 °C, corresponding to the decomposition of the main polymer, TMPTA. This peak indicates the onset of thermal curing, accompanied by a significant weight loss of approximately 10%. The thermal curing of TMPTA is crucial for achieving the desired material properties in the final ceramic product. No further apparent weight losses were observed beyond 550 °C, suggesting the complete removal of the organic additives at lower temperatures, and the complete thermal curing of TMPTA at higher temperatures. This multi-step heat-treatment approach ensures an efficient removal of the organics while allowing the desired ceramic material properties to develop. After debinding up to 800 °C in an inert atmosphere, a sintering at 1400 °C for 2 h in an oxidant atmosphere (synthetic Air) was carried out to fully densify the parts.

Using this fabrication methodology, ten 6Yb4ScSZ electrolytes consisting of a support ring of 1 cm diameter and a thin electrolyte membrane of 265 μm thick were produced (figure 2). As presented in the optical images of figure 2, crack-free cells with planar (figure 2(a)) and corrugated (figure 2(b)) architectures were successfully fabricated. Despite the similar projected area of the planar and corrugated button cells, the planar cells exhibited an active membrane area of 2.0 cm^2, while the corrugated cells presented an active area

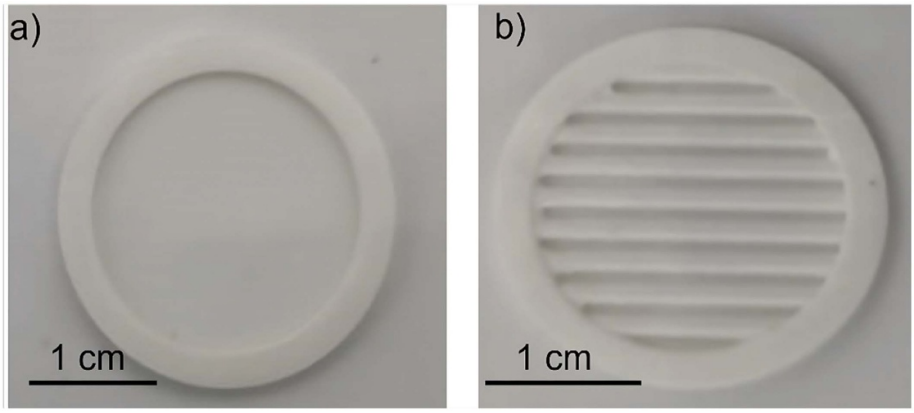

Figure 2. (a) Optical top view image of a planar 6Yb4ScSZ cell with an active area of ≈2 cm^2 (b) Optical top view image of a corrugated 6Yb4ScSz cell with an active area of ≈3.2 cm^2. Membrane thickness is 265 μm in both cases.

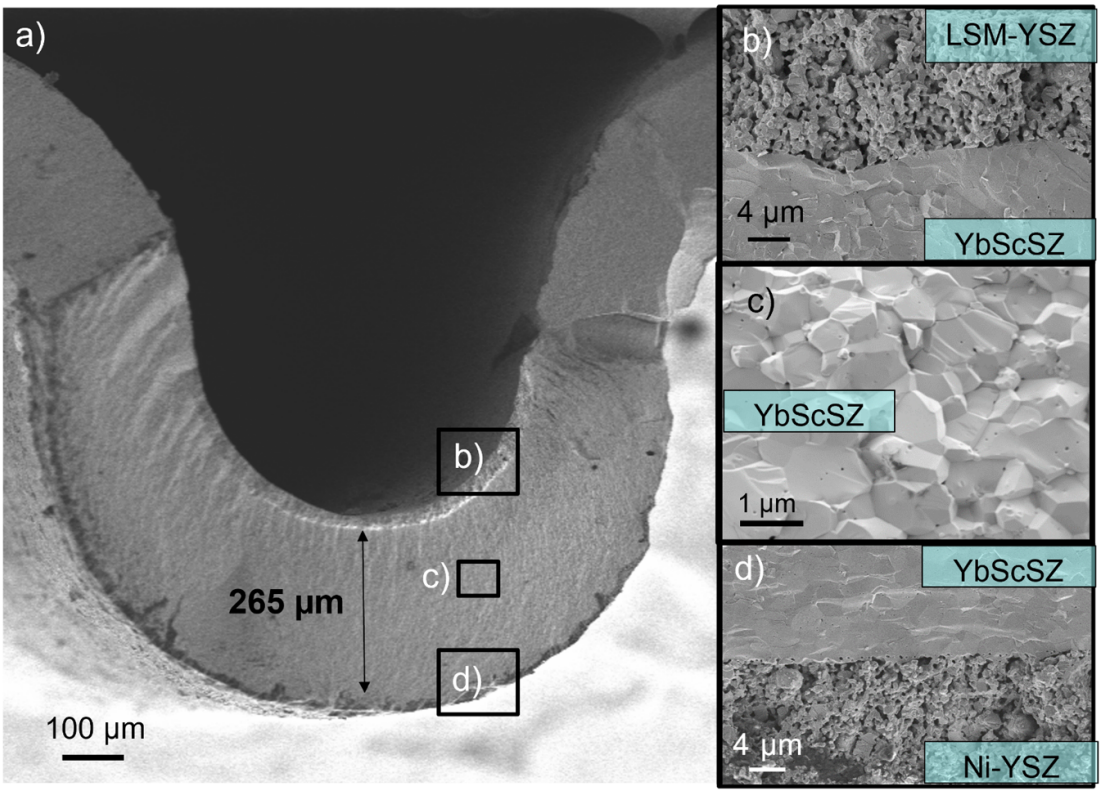

Figure 3. (a) SEM cross section of a corrugated cell showing the electrolyte thickness ≈265 μm (b) LSM-YSZ/6YbScSZ attachment, (c) the lower porosity present in the 6Yb4ScSZ electrolyte (d) the Ni-YSZ/6YbScSZ attachment.

of 3.2 cm^2, which represents a 60% increase. The sintered membranes of 6YbScSZ were further analyzed with XRD, (figure S1) confirming the stabilization of the cubic phase.

SEM images of the cross-section of the complete corrugated cells (figure 3(a)) and detailed pictures of the different layers and interfaces were acquired (LSM-YSZ in figure 3(b), 6Yb4ScSZ in figure 3(b) and Ni-YSZ in figure 3(c)). Figure 3(a) shows a homogeneous and dense thick electrolyte of 250–270 μm in thickness. A detail of the electrolyte (figure 3(c)), confirms a very high density with faceted grains and reduced amounts of small and closed porosity. Both electrodes (figures 3(b) and (d)), show and excellent homogeneity and the desired high porosity of the microstructure. Moreover, a good adhesion for the LSM-YSZ and Ni-YSZ to the 6Yb4ScSZ electrolyte is observed.

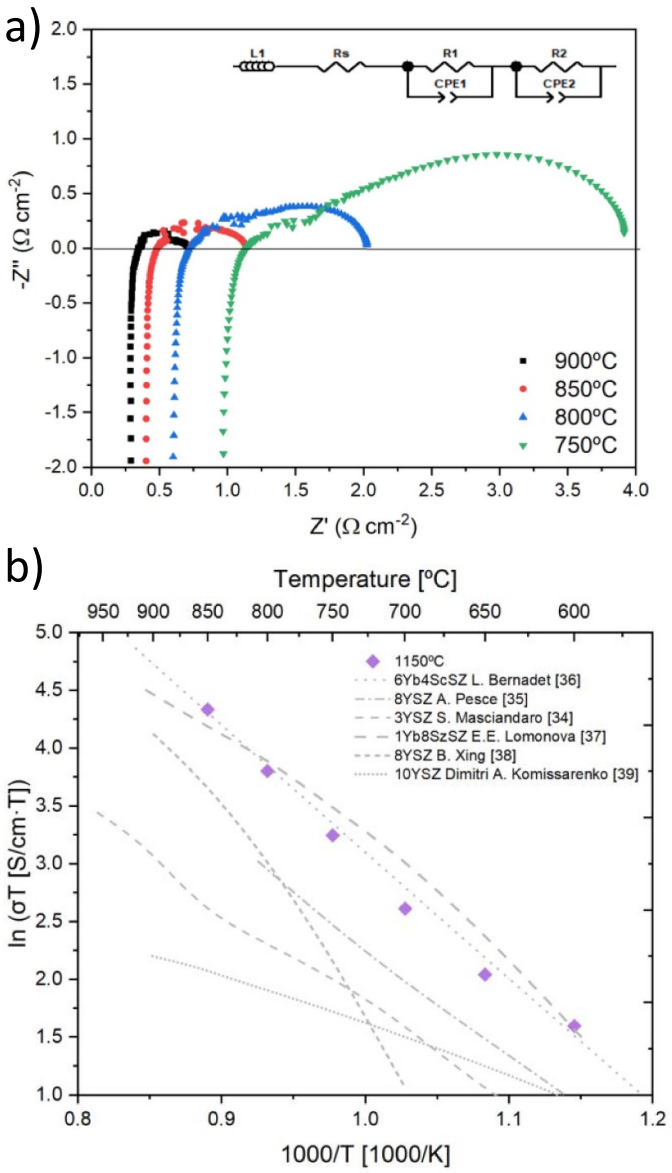

Figure 4. (a) Nyquist plot obtained for the cell with the temperature attachment of 1150 °C Arrhenius plot of the ionic conductivity of the 3D printed 6Yb4ScSZ obtained from the EIS measurements after deconvolution of the spectra. The solid line represents the experimental fitting of an Arrhenius behavior. Data from the literature as solid lines correspond to 6YbScSZ [35] 1Yb8ScSZ [36] 8YSZ 3D Printed electrolyte [34, 37] 10YSZ 3D Printed [38] and 3YSZ 3D printed electrolyte [33].

3.2. Electrochemical characterization of symmetrical cell

In order to confirm the electrochemical behavior of the fabricated electrolytes while optimizing the attachment temperature of the electrodes, symmetrical LSM-YSZ/6Yb4ScSz/LSM-YSZ planar cells with oxygen electrode sintered at different temperatures (1100 °C, 1150 °C 1200 °C respectively) were electrochemically characterized. EIS measurements were conducted in the temperature range of 500 °C–900 °C, exposing the cells to synthetic air in both sides. As an example, figure 4(a) shows the Nyquist plots measured for cells attached at 1150 °C and characterized at different temperatures from 750 °C to 900 °C. The equivalent circuit used for the fitting (inset figure 4(a)) is composed of an inductance (L_1), a serial resistance (R_s) and two ZARC elements ((R_iCPE_i), $i = 1,2$). After deconvolution of the impedance spectra employing the mentioned equivalent circuit, serial resistance values were obtained (figure S1). Cells attached at 1150 °C reported the lowest value of serial resistance and, therefore, were considered the optimal ones. For the optimized attachment temperature, one can associate the serial resistance mainly to the electrolyte resistance and estimate the ionic conductivity of the fabricated electrolyte (considering geometrical factors).

Figure 4(b) shows the Arrhenius plot of the estimated ionic conductivity of 6Yb4ScSZ as measured with optimized printed cells together with previously reported of the same material and values obtained for SoA

Table 2. Values of area-specific resistance (total, serial, and polarization contributions) obtained from equivalent circuit fitting of the EIS spectra for both planar and corrugated 6Yb4ScSz cells measured in SOFC (0.7 V) and SOEC (1.3 V) mode at 900 °C.

	SOFC mode (0.7 V)		SOEC mode (1.3 V)	
	ASR_{plan} (Ω $cm^{2)}$	ASR_{corr} (Ω $cm^{2)}$	ASR_{plan} (Ω $cm^{2)}$	ASR_{corr} (Ω $cm^{2)}$
Total	0.97	0.57	1.05	0.55
Serial	0.42	0.25	0.45	0.25
Polarization	0.55	0.32	0.6	0.3

YSZ electrolytes. The measured ionic conductivity of here fabricated 6Yb4ScSZ is 35 mS cm^{-1} at 850 °C, which is in good agreement with reported values from Bernadet *et al* (20 mS cm^{-1} at $T = 850$ °C) [35], showing an activation energy of 0.86 eV. Measured conductivity is notably higher than the one typically reported for 3YSZ and 8YSZ at the same temperature, about 0.5 mS cm^{-1} and 3 mS cm^{-1}, respectively [33, 34]. The obtained values of conductivity for the printed parts open the possibility of developing electrolyte-supported 3D printed cells based on this material able to operate at temperatures between 800 and 900 °C (accepted values of 0.5 Ω cm^{-2} are expected for 250 μm-thick electrolytes of 6Yb4ScSZ at 850 °C)

3.3. SOC performance in fuel cell and electrolysis modes

Employing the same 3D printed electrolytes; complete planar and corrugated cells (LSM-YSZ/6Yb4ScSZ/Ni-YSZ) were fabricated in order to evaluate their performance in SOFC and SOEC operation modes. Figures 5(a) and (b) show polarization curves of the complete cells in fuel cell and electrolysis modes, respectively, while figures 5(c) and (d) are devoted to present Nyquist plots of the EIS experiments carried out in the same conditions. First, polarization curves in fuel cell mode were measured at 900 °C using synthetic air and pure hydrogen atmosphere on the oxygen and fuel electrode chambers, respectively. Figure 5(a) shows the voltage–current (power) density curves for planar and corrugated cells measured in the indicated conditions. In the same plot, performance results for a 3D printed planar cell of 8YSZ [34] is also represented for comparison reasons. Open circuit voltage (OCV) values obtained for planar and corrugated cells were around 1.1 V, which are in agreement with the expected values calculated by the Nernst equation (1.11 V), confirming an adequate gas tightness of the printed electrolytes and cells. For the planar 6Yb4ScSz cell, a maximum power density of $p_p = 300$ mW cm^{-2} at 900 °C was obtained while, for the corrugated cell, a higher power density (per projected area) of $p_p = 470$ mW cm^{-2} at the same temperature. This increase represents a 60% enhancement, which straightforwardly corresponds to the 60% increase of the active area induced by design. In addition, the peak power density of the 6Yb4ScSZ planar cell can be compared to the 8YSZ cell counterpart resulting in an increase of 15%. Although this is a remarkable improvement, one would expect a higher enhancement (attending to the increase in one order of magnitude of the ionic conductivity of 6Yb4ScSZ compared to 8YSZ). In this regard, other serial resistances present in both systems such as current collectors and wires can partially hinder this enhancement by strongly dominating the behavior at this temperature. To better understand the different contributions to the total resistance of the different phenomena taking place, EIS measurements under typical SOFC operational voltages of 0.7 V were carried out and are represented in figure 5(c). The equivalent electrical circuit employed for fitting of the spectra is included in the inset of the figure. This circuit consists of an inductance (L), a resistance (R_S) representing the serial resistance and three ZARC elements in series. By data fitting using the equivalent circuit and normalization to the projected area, values of total area specific resistance (ASR) can be obtained for the planar, $ASR_{plan} = 0.97$ Ω cm^2, and corrugated, $ASR_{corr} = 0.57$ Ω cm^2, cells. These total ASR values can be split into a serial resistance (ASRs), referring to the contribution of the electrolyte and current collectors, and the polarization resistance (ASRp), typically associated with the contribution of the different phenomena occurring at the electrodes. For planar cells, values of ASRs = 0.42 Ω cm^2 and ASRp = 0.55 Ω cm^2 were obtained while, for the corrugated ones, lower values of ASRs = 0.25 Ω cm^2 and ASRp = 0.35 Ω cm^2 were measured, as expected (see table 2).

After SOFC characterization, the complete cell was also tested under electrolysis mode at the same temperature but employing synthetic air and steam water as atmospheres. Figure 5(b) shows the voltage-current (power) density curves for the planar and corrugated 6Yb4ScSZ cells and the reference 8YSZ 3D-printed cells from [34]. In analogy with the analysis of the SOFC results, reasonable OCV values were obtained for planar and corrugated cells (OCV ca. 0.8 V compared to expected values of 0.83 V). Maximum injected current densities of -600 mA cm^{-2} at 1.4 V were obtained for planar cells while a remarkable injection current of -1 A cm^{-2} was reached at the same voltage by the corrugated cell (representing a 63% increase compared to the planar configuration). Compared to values of -480 mA cm^2 reported for the planar 8YSZ counterpart [34], 6Yb4ScSZ planar cells showed a notable improvement in performance (25%).

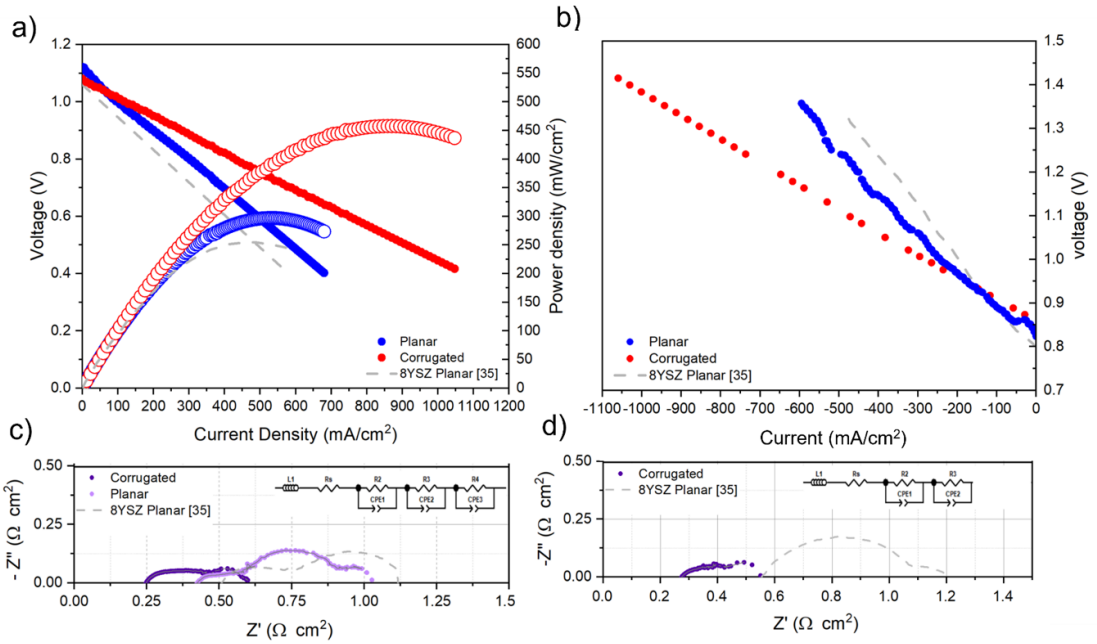

Figure 5. V–j 3D printed 6Yb4ScSZ planar and corrugated button cells measured in SOFC (a) and electrolysis (b) at 900 °C. Correlated Nysquits plots from EIS measurements for a typical operating voltage of 0.7 V for SOFC and 1.3 V for SOEC. The dashed line represents the experimental data obtained during the measurements and the solid line data from the literature (Pesce et al [34]).

Similar to the EIS analysis carried out in SOFC mode, Nyquist plots (figure 5(d)) and deconvolution of the different contributions using equivalent circuits allowed obtaining values of $ASR_{plan} = 1.05\ \Omega\ cm^2$ and ASR_{corr} 0.55 Ω cm^2 at voltages characteristics of the SOEC mode ($V = 1.3$ V). Splitting the contributions from the ohmic and polarization contributions, ASRs = 0.45 Ω cm^2 and ASRp = 0.60 Ω cm^2 were obtained for the planar cell and ASRs = .25 Ω cm^2 and ASRp = 0.35 Ω cm^2 for the corrugated cell (see table 2).

After performance of the cells was measured and evaluated, mid-term tests were carried out for the corrugated 6Yb4ScSz cell in SOFC mode at 850 °C (for more details see supplementary info figure S2). Figure 6 presents the voltage evolution over time during a galvanostatic test using a current density of $I = -440$ mA cm^2 at 850 °C. A standard conditioning time of 150 h [39]was considered to ensure a stable performance. After voltage stabilization, the voltage evolution of the corrugated cell was monitored for a period of 350 h. The cell showed a degradation rate of 1.65 mV 1000 h^{-1}, equivalent to a degradation rate of 0.22% 1000 h^{-1}, which could be considered a low degradation according to the methods and materials used in this work. SEM characterization was done to the aged cell after 350 h, figure 7(a) shows the LSM electrolyte interface and figure 7(b) shows the 6Yb4ScSZ electrolyte, no apparent changes can be observed before the aging time.

4. Conclusions

In this work, SLA 3D printing of 6Yb4ScSz has been developed to produce complex-shape electrolytes for SOC applications with better performance than counterparts based on state-of-the-art 8YSZ. Fully dense and crack-free 6Yb4ScSz electrolytes of 265 μm in thickness were reliably fabricated and electrochemically characterized reaching ionic conductivity as high as 0.035 S cm^{-2} at 850 °C. Employing such 3D printing approach, planar and corrugated electrolyte-supported SOC made of LSM-YSZ/6Yb4ScSZ/Ni-YSZ were successfully produced. Planar cells presented a remarkable performance in both fuel cell and electrolysis mode, improving results obtained using 8YSZ electrolytes. A peak power density of 300 mW cm^{-2} and a maximum injected current of −600 mA cm^{-2} (at 1.3 V) were obtained in SOFC and SOEC modes, respectively, at 900 °C. More interestingly, corrugated 6Yb4ScSZ cells presented enhanced values of peak power density and maximum injected current of 470 mW cm^{-2} and 1 A cm^{-2}, respectively, which directly correspond to the increase in active area induced by design. In addition, mid-term galvanostatic operation tests carried out under SOFC conditions ($I = -433$ mA cm^2 at 850 °C for more than 500 h) demonstrated that corrugated printed cells based on 6YbScSZ are very stable and can be competitive with currently existing technologies. These results can be considered the first step to investigate complex-shape SOC cells based on unconventional materials, which will open the way to operate at lower temperatures and with higher

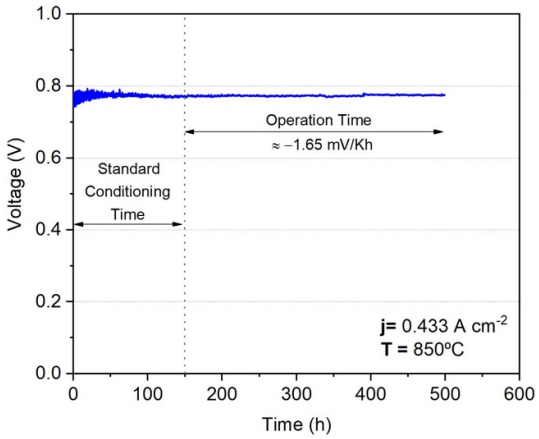

Figure 6. Mid-term stability test carried out during 500 h for a corrugated cell measured at 850 °C and a fixed current of I = 433 mA cm^{-2}. A period of 100 h of stabilization and a later degradation period of 400 h.

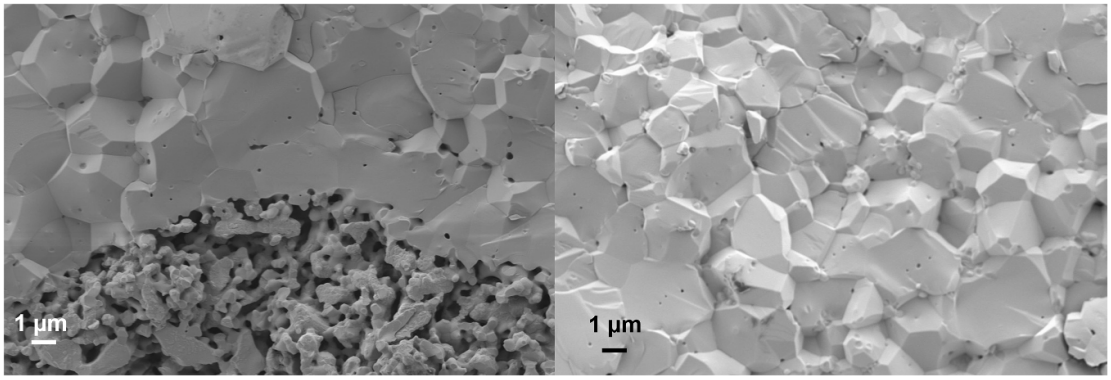

Figure 7. (a)SEM picture of LSM-6Yb4ScSZ interface after an operation time of 450 h (b) 6YbScSZ aspect after an operation time of 450 h.

performances. Furthermore, the obtained and discussed performance stability in SOFC mode foreshadows the future impact of this technology impact for real-world applications, especially when compared to conventional manufacturing procedures, as recently described by the authors [39].

Data availability statement

The data that support the findings of this study are openly available at the following URL/DOI: https://zenodo.org/communities/hyp3d/?page=1&size=20.

Acknowledgments

This project has received funding from the Fuel Cells and Hydrogen Joint Undertaking (now Clean Hydrogen Partnership) under Grant Agreement No. 101101274 (HYPE3D) and also the support The Joint Undertaking receives support from the European through the frame of RETOS call for the TED2021-131267B-C31 (SIMPEL) and also the support through the frame of RETOS call for the PID2019-107106RB-C31 (3D-Progress).

ORCID iDs

Santiago Márquez https://orcid.org/0000-0003-3627-2318
Simone Anelli https://orcid.org/0000-0002-5693-0464
Maritta Lira https://orcid.org/0000-0002-1315-4346
Antonio Maria Asensio https://orcid.org/0000-0003-4390-0212

Marc Torrell https://orcid.org/0000-0002-3946-1352
Albert Tarancón https://orcid.org/0000-0002-1933-2406

References

[1] da Graça Carvalho Maria 2012 EU energy and climate change strategy *Energy* **40** 12–22
[2] Abe J O, Popoola A P I, Ajenifuja E and Popoola O M 2019 Hydrogen energy, economy and storage: review and recommendation *Int. J. Hydrog. Energy* **44** 15072–86
[3] Gross R, Leach M and Bauen A 2003 Progress in renewable energy (available at: www.elsevier.com/locate/envint)
[4] Chen H, Cong T N, Yang W, Tan C, Li Y and Ding Y 2009 Progress in electrical energy storage system: a critical review *Prog. Nat. Sci.* **19** 291–312
[5] Dodds P E, Staffell I, Hawkes A D, Li F, Grünewald P, McDowall W and Ekins P 2015 Hydrogen and fuel cell technologies for heating: a review *Int. J. Hydrog. Energy* **40** 2065–83
[6] Jain I P 2009 Hydrogen the fuel for 21st century *Int. J. Hydrog. Energy* **34** 7368–78
[7] I.—International Energy Agency 2022 Global hydrogen review 2022 (available at: www.iea.org/t&c/)
[8] Parkinson B, Balcombe P, Speirs J F, Hawkes A D and Hellgardt K 2019 Levelized cost of CO_2 mitigation from hydrogen production routes *Energy Environ. Sci.* **12** 19–40
[9] Safari F and Dincer I 2020 A review and comparative evaluation of thermochemical water splitting cycles for hydrogen production *Energy Convers. Manage.* **205** 112182
[10] Jafari T, Moharreri E, Amin A S, Miao R, Song W and Suib S L 2016 Photocatalytic water splitting—The untamed dream: a review of recent advances *Molecules* **21** 900
[11] Ni M, Leung M K H and Leung D Y C 2008 Technological development of hydrogen production by solid oxide electrolyzer cell (SOEC) *Int. J. Hydrog. Energy* **33** 2337–54
[12] Zhang J *et al* 2006 High temperature PEM fuel cells *J. Power Sources* **160** 872–91
[13] Zeng K and Zhang D 2010 Recent progress in alkaline water electrolysis for hydrogen production and applications *Prog. Energy Combust. Sci.* **36** 307–26
[14] Boldrin P and Brandon N P 2019 Progress and outlook for solid oxide fuel cells for transportation applications *Nat. Catal.* **2** 571–7
[15] Milewski J, Wejrzanowski T, Szabłowski Ł, Baron R, Szczęśniak A and Ćwieka K 2017 Development of molten carbonate fuel cells at warsaw university of technology *Energy Proc.* **142** 1496–501
[16] Blum L, Meulenberg W A, Nabielek H and Steinberger-Wilckens R 2010 Worldwide SOFC technology overview and benchmark (available at: www.ceramics.org/ACT)
[17] Vinchhi P, Khandla M, Chaudhary K and Pati R 2023 Recent advances on electrolyte materials for SOFC: a review *Inorg. Chem. Commun.* **152** 110724
[18] Badwal S P S, Ciacchi F T and Milosevic D 2000 Scandia-zirconia electrolytes for intermediate temperature solid oxide fuel cell operation (available at: www.elsevier.com/locate/ssi)
[19] Haering C, Roosen A, Schichl H and Schnöller M 2005 Degradation of the electrical conductivity in stabilised zirconia system Part II: scandia-stabilised zirconia *Solid State Ion.* **176** 261–8
[20] Yamamoto O *et al* 1995 Electrical conductivity of stabilized zirconia with ytterbia and scandia *Solid State Ion.* **79** 137–42
[21] Vijaya Lakshmi V and Bauri R 2011 Phase formation and ionic conductivity studies on ytterbia co-doped scandia stabilized zirconia ($0.9ZrO_2$-$0.09Sc_2O_3$-0. $01Yb_2O_3$) electrolyte for SOFCs *Solid State Sci.* **13** 1520–5
[22] Yildiz E, Yilmaz S and Turkoglu O 2016 The production and characterization of ytterbium-stabilized zirconia films for SOFC applications *Int. J. Appl. Ceram Technol.* **13** 100–7
[23] Connor P A *et al* 2018 Tailoring SOFC electrode microstructures for improved performance *Adv. Energy Mater.* **8** 1800120
[24] O'Hayre R, Barnett D M and Prinz F B 2005 The triple phase boundary *J. Electrochem. Soc.* **152** A439
[25] Lu X, Heenan T M M, Bailey J J, Li T, Li K, Brett D J L and Shearing P R 2017 Correlation between triple phase boundary and the microstructure of solid oxide fuel cell anodes: the role of composition, porosity and Ni densification *J. Power Sources* **365** 210–9
[26] O'Hayre R, Cha S-W, Colella W and Prinz F B 2016 Front Matter *Fuel Cell Fundamentals* (Wiley) pp i–xx
[27] Minh N Q 1993 Ceramic fuel cells *J. Am. Ceram. Soc.* **563** 88
[28] Nishihora R K, Rachadel P L, Quadri M G N and Hotza D 2018 Manufacturing porous ceramic materials by tape casting—a review *J. Eur. Ceram Soc.* **38** 988–1001
[29] Jabbari M, Bulatova R, Tok A I Y, Bahl C R H, Mitsoulis E and Hattel J H 2016 Ceramic tape casting: a review of current methods and trends with emphasis on rheological behaviour and flow analysis *Mater. Sci. Eng.* B **212** 39–61
[30] Hsieh W S, Lin P and Wang S F 2013 Fabrication of electrolyte supported micro-tubular SOFCs using extrusion and dip-coating *Int. J. Hydrog. Energy* **38** 2859–67
[31] Du Y, Sammes N M and Tompsett G A 1200 Optimisation parameters for the extrusion of thin YSZ tubes for SOFC electrolytes
[32] Tarancón A *et al* 2022 2022 roadmap on 3D printing for energy *J. Phys. Energy* **4** 011501
[33] Masciandaro S, Torrell M, Leone P and Tarancón A 2019 Three-dimensional printed yttria-stabilized zirconia self-supported electrolytes for solid oxide fuel cell applications *J. Eur. Ceram. Soc.* **39** 9–16
[34] Pesce A, Hornés A, Núñez M, Morata A, Torrell M and Tarancón A 2020 3D printing the next generation of enhanced solid oxide fuel and electrolysis cells *J. Mater. Chem.* A **8** 16926–32
[35] Bernadet L, Moncasi C, Torrell M and Tarancón A 2020 High-performing electrolyte-supported symmetrical solid oxide electrolysis cells operating under steam electrolysis and co-electrolysis modes *Int. J. Hydrog. Energy* **45** 14208–17
[36] Lomonova E E *et al* 2020 ZrO_2–Sc_2O_3 solid electrolytes doped with Yb_2O_3 or Y_2O_3 *Russ. J. Electrochem.* **56** 118–23
[37] Xing B, Cao C, Zhao W, Shen M, Wang C and Zhao Z 2020 Dense 8 mol% yttria-stabilized zirconia electrolyte by DLP stereolithography *J. Eur. Ceram. Soc.* **40** 1418–23
[38] Komissarenko D A, Sokolov P S, Evstigneeva A D, Slyusar I V, Nartov A S, Volkov P A, Lyskov N V, Evdokimov P V, Putlayev V I and Dosovitsky A E 2021 DLP 3D printing of scandia-stabilized zirconia ceramics *J. Eur. Ceram. Soc.* **41** 684–90
[39] Ferreira V J, Wolff D, Hornés A, Morata A, Torrell M, Tarancón A and Corchero C 2021 5 kW SOFC stack via 3D printing manufacturing: an evaluation of potential environmental benefits *Appl. Energy* **291** 116803